Progress in Elementary Processes for Negative Ion Source Modeling

M. Capitelli[†*], M. Cacciatore[†], R. Celiberto[**], F. Esposito[†], A. Laricchiuta[†] and M. Rutigliano[†]

[*]*Dipartimento di Chimica Università di Bari, Italy*
[†]*IMIP, Sezione di Bari, CNR, Italy*
[**]*Dipartimento di Ingegneria Civile ed Ambientale, Politecnico di Bari, Italy*

Abstract. Cross sections for elementary processes relevant in the modeling of negative ion sources are reviewed, with particular attention to the dependence on the vibrational excitation of the target molecule. Electron impact induced excitation and dissociation processes in H_2 molecule and its isotopic variants are considered. Ro-vibrationally resolved cross sections for dissociation and de-excitation occurring in atom-molecule collision processes are presented. Finally the theoretical determination of hydrogen recombination probability on graphite surface is also considered.

INTRODUCTION

A great effort has been devoted in the last decade to the theoretical characterization of negative ion sources, emphasizing the role of non-equilibrium in enhancing the negative ion production [1, 2].

Dissociative attachment is recognized as the main channel for H^- production

$$H_2(X^1\Sigma_g^+, v_i) + e \rightarrow H_2^- \rightarrow H + H^- \tag{1}$$

The efficiency of this process is greatly enhanced by vibrational excitation of molecular target [3, 4], therefore, in order to optimize the source operating conditions, the knowledge of all the elementary processes affecting the vibrational distribution, destroying excited states or populating vibrational levels, is of paramount importance.

Furthermore extraordinarily high rate of H^- formation has been observed, in particular experimental conditions [12], opening question about the relevance of alternative mechanisms involving highly excited Rydberg states.

In this frame processes involving vibrationally as well as electronically excited H_2 molecule are characterized through the corresponding state-resolved cross sections, being these data relevant for both kinetic modeling of negative ion sources [5] and experimental diagnostic methods [6].

Electron-molecule collision processes have been extensively studied [7] due to their efficiency in affecting the H_2 distribution on the internal degrees of freedom. Also heavy collisions act in the plasma promoting dissociation and energy redistribution in the vibrational ladder. Finally the catalytic activity of source's walls in recombination processes determine a nascent vibrational distribution with a strong non-Boltzmann character.

In this paper a review of the work done on elementary processes by the plasma chemistry group of Bari is presented.

ELECTRON-MOLECULE COLLISION PROCESSES

Electronic excitation Allowed transitions to the singlet terms of the H_2 spectrum promoted by electron impact have been widely investigated, representing the first step of the indi-

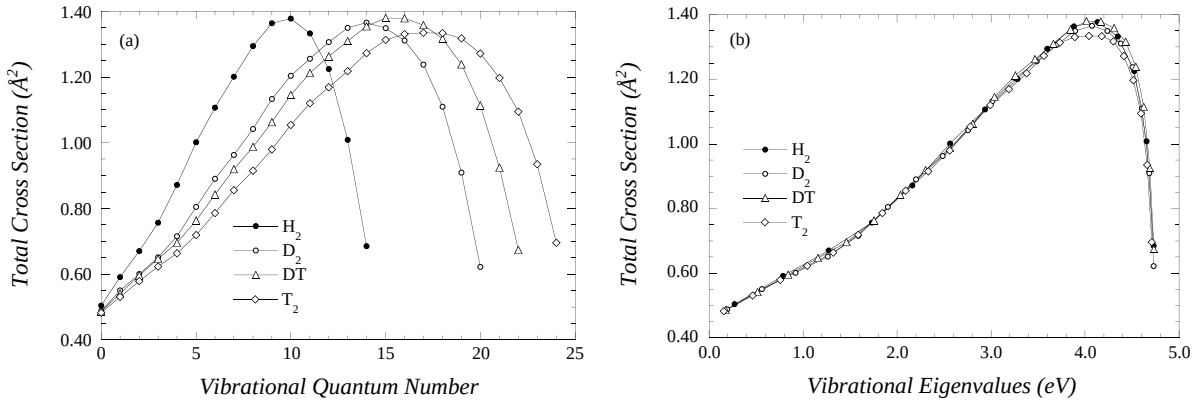

FIGURE 1. Cross section for the transition $(X^1\Sigma_g^+, v_i) \rightarrow (B^1\Sigma_u^+)$ for different isotopes, at a fixed energy of 40 eV, (a) as a function of initial vibrational quantum number; (b) as a function of vibrational eigenvalues.

rect mechanism of vibrational excitation, the so-called *E-V process*

$$H_2(X^1\Sigma_g^+, v_i) + e \rightarrow H_2^*(\textit{excited singlet states}) \rightarrow H_2(X^1\Sigma_g^+, v_f) + e + h\nu. \tag{2}$$

As sketched the fate of excited states is to radiatively decay back to the ground electronic state populating preferentially the high vibrational levels (v_f).

The principal excitations in this excitation-radiative sequence proceed through the lowest singlets $B^1\Sigma_u^+$ and $C^1\Pi_u$ [10]

$$H_2(X^1\Sigma_g^+, v_i) + e \rightarrow H_2(B^1\Sigma_u^+) + e \tag{3}$$

$$H_2(X^1\Sigma_g^+, v_i) + e \rightarrow H_2(C^1\Pi_u) + e \tag{4}$$

Total cross sections (summed over final bound and continuum vibrational states) for the processes (3),(4), calculated in the framework of the semiclassical impact-parameter method, have been reported in refs. [8, 9, 7] for H_2, D_2, T_2 and DT molecules, as function of both the collision energy and the initial vibrational quantum number. These results allow an interesting study on the existence of isotopic effect. In figure 1a the dependence of total cross section on the initial vibrational quantum number for the $X \rightarrow B$ excitation process is presented, at a fixed incident energy, for all isotopic variants of hydrogen molecule. The observed shift of cross sections to higher values of v_i, in passing from H_2 to T_2 molecule, seems to correspond to the increase of molecular mass. However this isotopic effect is only apparent and the cross sections collapse if plotted as a function of the vibrational eigenvalues (figure 1b), suggesting a dependence of excitation cross section on the vertical transition energy.

A not negligible contribution in process (2) is also represented by radiative cascade processes from higher singlet states [10]. Excitations to the B', B'', D, D' states, usually referred as low-lying Rydberg states, have been also studied [11]

$$H_2(X^1\Sigma_g^+, v_i) + e \rightarrow H_2(B'^1\Sigma_u^+) + e \tag{5}$$

$$H_2(X^1\Sigma_g^+, v_i) + e \rightarrow H_2(B''^1\Sigma_u^+) + e \tag{6}$$

$$H_2(X^1\Sigma_g^+, v_i) + e \rightarrow H_2(D^1\Pi_u) + e \tag{7}$$

$$H_2(X^1\Sigma_g^+, v_i) + e \rightarrow H_2(D'^1\Pi_u) + e \tag{8}$$

Total cross sections for processes (5)-(8) are presented in figure 2a-d, respectively.

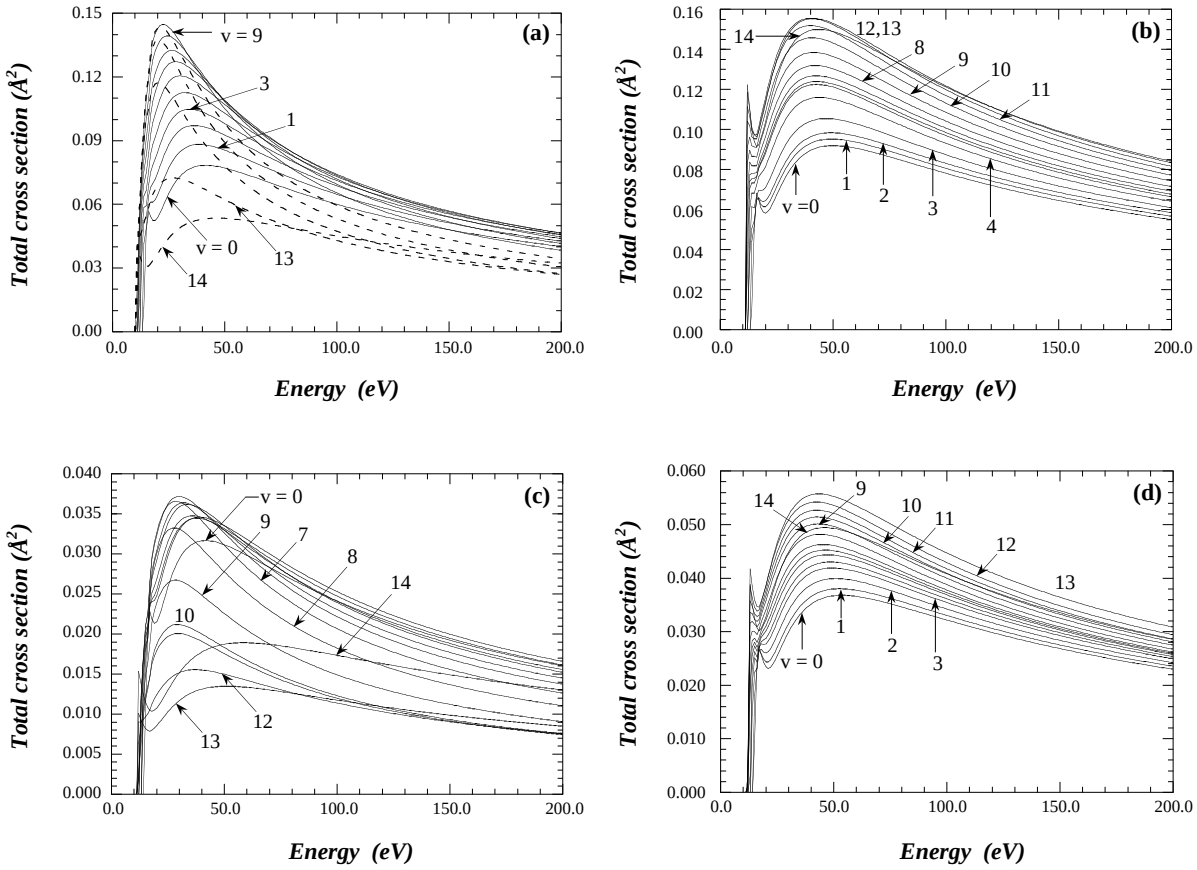

FIGURE 2. Cross section as a function of energy, for different initial vibrational levels, for the process: (a) $H_2(X^1\Sigma_g^+, v_i) + e \rightarrow H_2(B^{'\,1}\Sigma_u^+) + e$; (b) $H_2(X^1\Sigma_g^+, v_i) + e \rightarrow H_2(D^1\Pi_u) + e$; (c) $H_2(X^1\Sigma_g^+, v_i) + e \rightarrow H_2(B^{"\,1}\Sigma_u^+) + e$; (d) $H_2(X^1\Sigma_g^+, v_i) + e \rightarrow H_2(D^{'\,1}\Pi_u) + e$.

Dissociation The forbidden transition from the ground state to the pure repulsive $b^3\Sigma_u^+$ state represents the main dissociative channel and the related cross sections, for different initial vibrational quantum numbers, have been calculated by different authors [13, 14, 7]. As expected in forbidden transitions the $X \rightarrow b$ cross section is peaked in the threshold region, while in the high energy region the allowed transitions to the continuum of bound excited electronic states give a significant contribution.

A global dissociative cross section for direct dissociation through excited singlets, including Rydberg states, is reported in figure 3. The irregular dependence on the initial vibrational quantum number, determined by the behaviour of Franck Condon density [15, 11], shows that the dissociation is favoured by vibrational excitation.

Transitions populating the vibrational manifold of the lowest bound triplet states (processes (9),(10)) also lead to dissociation through radiative cascade to the b state and predissociation mechanisms, respectively.

$$H_2(X^1\Sigma_g^+, v_i) + e \rightarrow H_2(a^3\Sigma_g^+, v') + e \tag{9}$$

$$H_2(X^1\Sigma_g^+, v_i) + e \rightarrow H_2(c^3\Pi_u, v') + e \tag{10}$$

State-to-state excitation cross sections, obtained in the Born approximation, summed on the final vibrational manifold, are reported in figure 4a-b. The direct dissociation through these states is negligible, this being confirmed by the Franck Condon density evaluation.

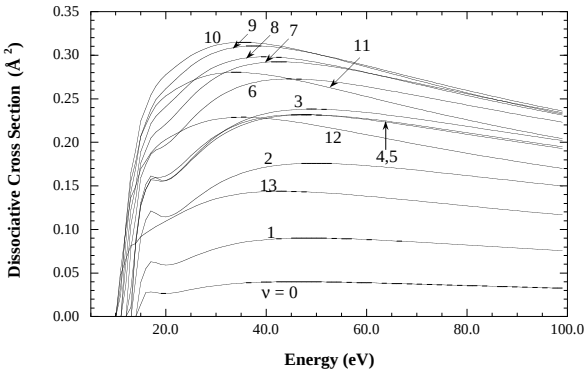

FIGURE 3. Cross section as a function of energy, for different initial vibrational levels, for the process: $H_2(X^1\Sigma_g^+, v_i) + e \rightarrow H_2(B, B', B''^1\Sigma_u^+; C, D, D'^1\Pi_u) + e \rightarrow H + H + e$.

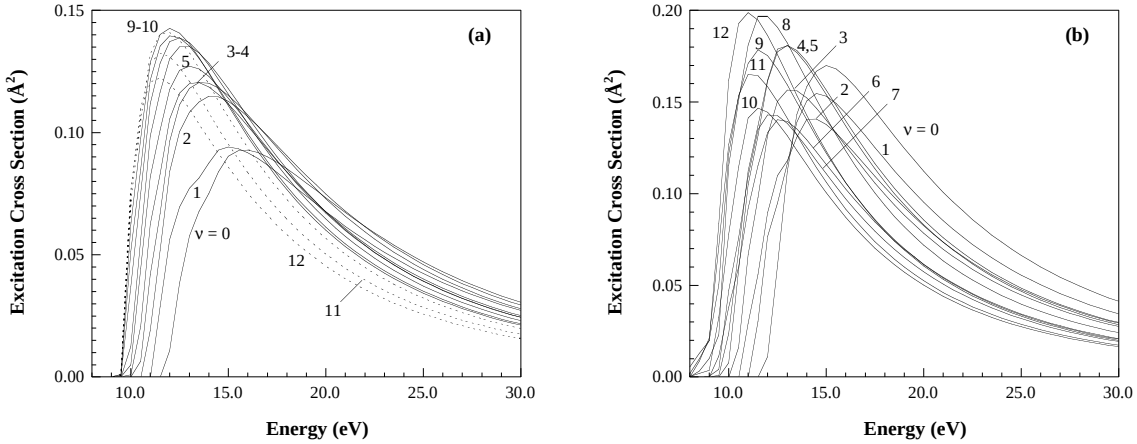

FIGURE 4. Cross sections as a function of energy for the process (a) $H_2(X^1\Sigma_g^+, v_i) + e \rightarrow H_2(a^3\Sigma_g^+) + e$; (b) $H_2(X^1\Sigma_g^+, v_i) + e \rightarrow H_2(c^3\Pi_u) + e$.

Triplet-triplet transitions Only few examples of cross section calculations involving two electronically excited states are available in literature [7], nevertheless these transition can be relevant in plasma modeling. Transitions initiated from the metastable $a^3\Sigma_g^+$ and $c^3\Pi_u$ states to other excited triplet states of H_2 molecules have been considered [16]. In particular process (11), known as Fulcher transition, is important in spectroscopic diagnostic methods, providing information about vibrational and rotational population of hydrogen plasmas [6].

$$H_2(a^3\Sigma_g^+, v_i) + e \rightarrow H_2(d^3\Pi_u) + e \tag{11}$$

$$H_2(c^3\Pi_u, v_i) + e \rightarrow H_2(g^3\Sigma_g^+) + e \tag{12}$$

$$H_2(c^3\Pi_u, v_i) + e \rightarrow H_2(h^3\Sigma_g^+) + e \tag{13}$$

Total cross sections for transitions (11),(12) are shown, as a function of collision energy, respectively in figure 5a,b. The relative position of potential energy curves for electronic states does not favour the dissociative channel, which represents a negligible contribution to the total cross sections.

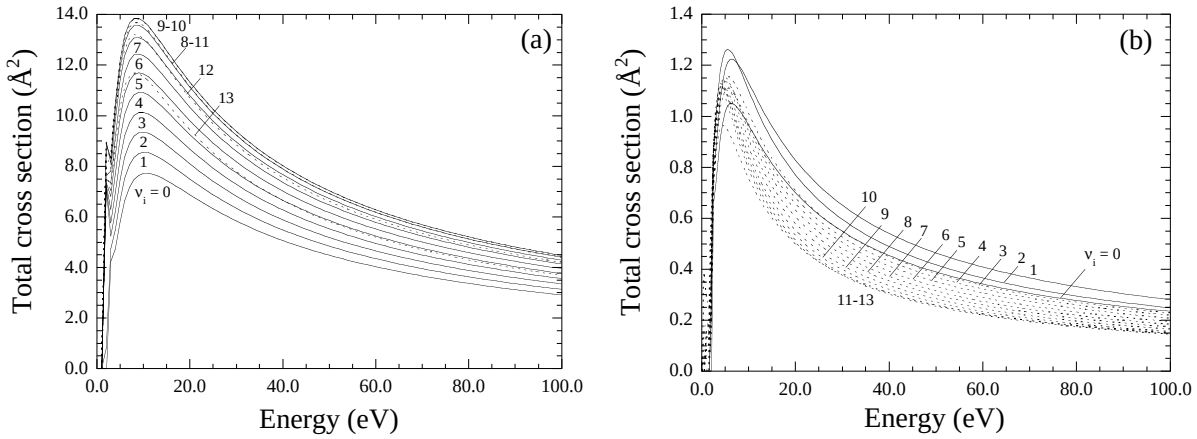

FIGURE 5. Cross sections as a function of energy for the process (a) $H_2(a^3\Sigma_g^+, v_i) + e \rightarrow H_2(d^3\Pi_u) + e$; (b) $H_2(c^3\Pi_u, v_i) + e \rightarrow H_2(g^3\Sigma_g^+) + e$.

A special treatment is required for the transition to the $h^3\Sigma_g^+$ state, whose adiabatic potential energy curve exhibits a barrier sustaining three quasi-bound vibrational levels (figure 6). These vibrational states, due to their quasistationary character, can lead to dissociation tunneling through the barrier

Energy positions of quasi-bound vibrational states is determined by using the method of *internal amplitude, (IA)*, defined as

$$IA(\varepsilon) = \int_{R_a}^{R_b} \frac{|\Psi_\varepsilon(R)|^2 \, dR}{[R_b - R_a]} \tag{14}$$

(R_a and R_b are the two classical turning points of the vibrational ε energy level). The IA is shown in figure 7 as a function of the potential energy ε. The peaks indicate three regions of resonances which, except for the last one very close to the top of the barrier, present a very sharp intensity. At a closer resolution becomes evident the energy enlargement, as shown in the inserted picture in figure 7. In figure 6 are shown the vibrational wavefunctions of three quasi-bound states, at a selected energy corresponding to the maximum of the related IA. In the same plot the dotted line represent, as a comparison, the wavefunction of completely dissociative state. The cross sections for these states depend on the ratio between the tunneling and radiative times. The calculated values (obtained by evaluating the tunneling probabilities and radiative Einstein coefficients) are shown in figure 8. As expected, the last resonance, located at the maximum of the barrier, shows a strong dissociative character, being the contrary for the first state, placed inside the potential well, which behaves practically as a bound state. An ibrid character is displayed by the second resonance.

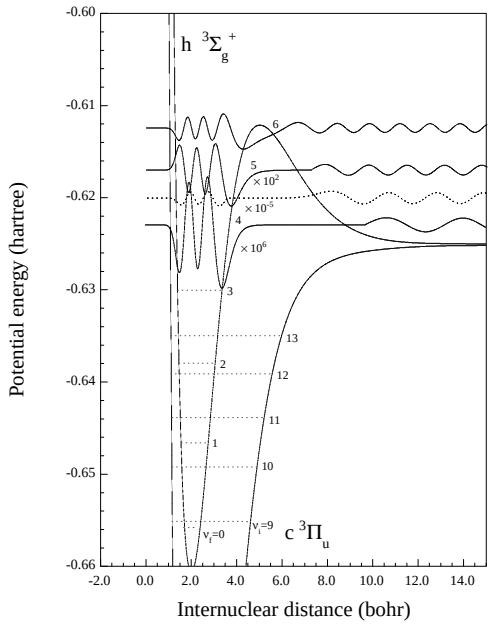

FIGURE 6. Potential energy curves and vibrational levels for $c^3\Pi_u$ and $h^3\Sigma_g^+$ states of H_2. Some wavefunctions of quasi-bound states (corresponding to Internal Amplitude peaks) (full lines) and for a non quasi-bound level (dashed line) are also displayed. The left portion of the first three wavefunctions (from the origin of the internuclear distance to the right wall of the barrier) has been multiplied by 10^{-6}, 10^5 (dashed line) and 10^{-2} for a better representation.

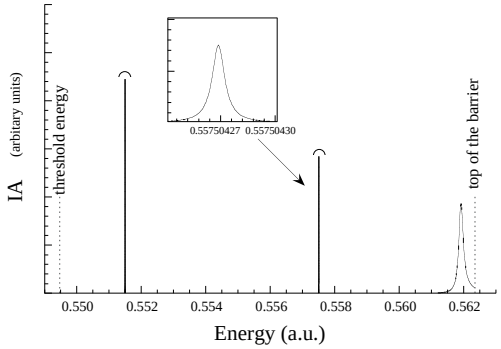

FIGURE 7. Internal amplitude (14) as a function of continuum energy (the second peak is magnified in the inserted picture)

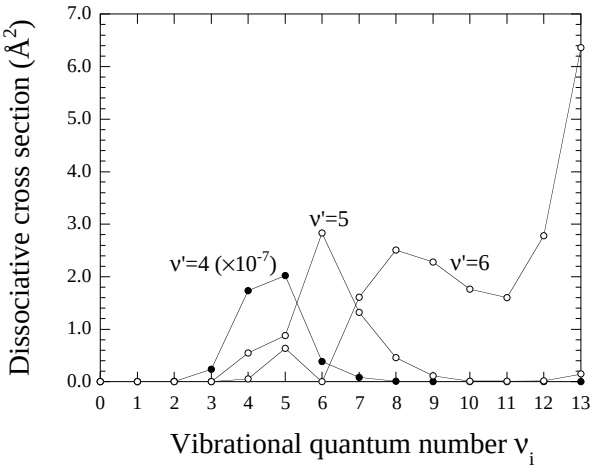

FIGURE 8. Quasi-bound state dissociative cross section for the process $H_2(c^3\Pi_u, v_i) + e \rightarrow H_2(h^3\Sigma_g^+, v') + e$ as a function of initial vibrational quantum number, at the incident energy E=10 eV. The curve labeled as $v' = 4$ has been multiplied by a factor of 10^7.

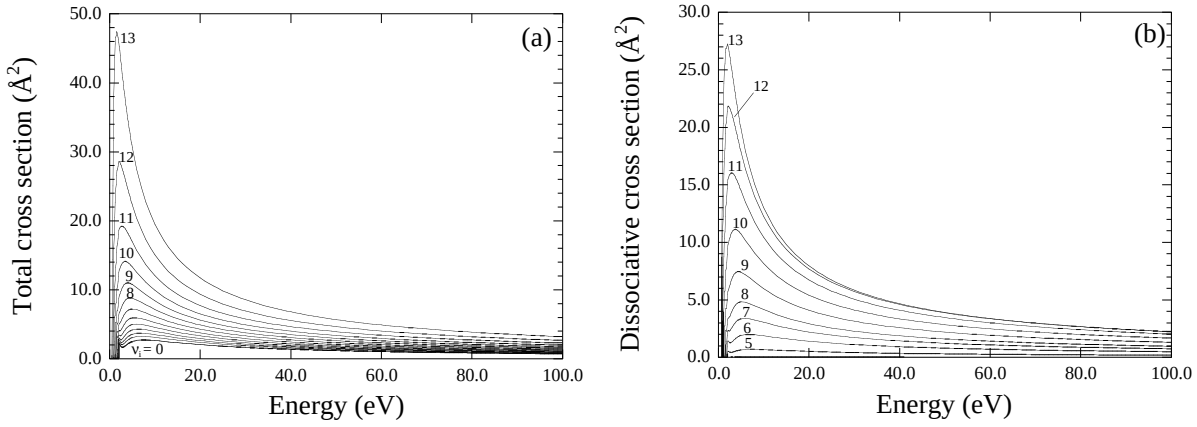

FIGURE 9. Cross sections as a function of energy for the process (a) $H_2(c^3\Pi_u, v_i) + e \rightarrow H_2(h^3\Sigma_g^+) + e$; (b) $H_2(c^3\Pi_u, v_i) + e \rightarrow H_2(h^3\Sigma_g^+, v) + e \rightarrow H + H + e$.

Total and dissociative cross sections for $c \rightarrow h$ transition, as a function of the energy and the initial vibrational quantum number, are presented in figure 9.

ATOM-MOLECULE COLLISION PROCESSES

Extensive dynamical calculations have been performed [17] on the LSTH (Liu-Siegbahn-Truhlar-Horowitz) PES [18] of state-to-state (*VT-processes*) and dissociation cross sections for collision of atomic hydrogen with rovibrationally excited molecular hydrogen.

All possible molecular rovibrational states (348) relative to the used PES have been considered and used as initial states, including quasibound ones (classically bound but quantally subject to tunnelling), which are of importance for recombination kinetics [19].

The code integrates the Hamilton equations of motion using Runge-Kutta fourth-order method with variable time step size controlled by a space interval of 0.015 Åand a velocity interval of 0.01 Å/fs. Total energy error checks (6×10^{-4} eV) are also performed. The impact parameter is scanned using a stratified sampling method. The standard QCT method (quasiclassical trajectory method) has been modified by using continuous distributions of rovibrational actions in reactants instead of delta function distributions, weighting trajectories with a simple "square window" function centered in integer values with integer width [20].

Dissociative cross sections as a function of the relative collision energy for different (v,j) pairs are presented in figure 10.

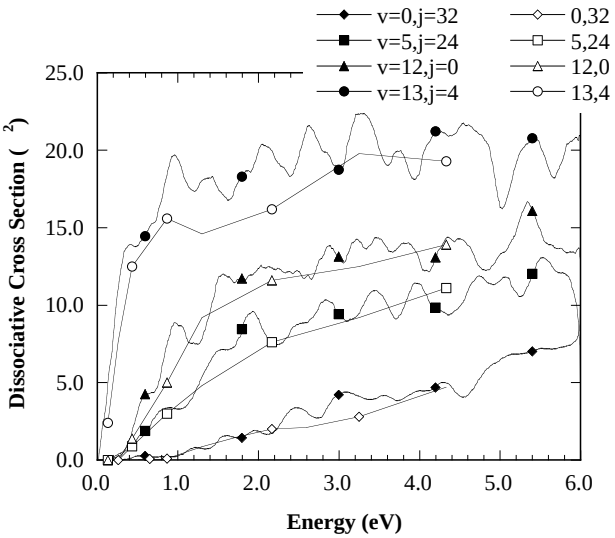

FIGURE 10. Dissociative cross section for selected initial states of H_2, as a function of collision energy, compared with results of ref. [21] (open symbols).

Cross section energy profile is characterized by a threshold energy, decreasing with the target internal energy, and by an increasing trend up to a maximum, whose value strongly depends on the initial roto-vibrational state. Comparing the cross sections with results calculated with a similar approach for few transitions by Dove and Mandy [21] (also reported in figure 10) a good agreement is found.

State-selected dissociative rate coefficients, $K_d(v)$, (figure 11) have been obtained from cross section data, averaging on a Boltzmann distribution function of the rotational states.

Cross sections for vibrational de-excitation process

$$H + H_2(v, T_{rot}) \rightarrow H + H_2(v', all\, j') \tag{15}$$

summed over final j' values and averaged on the rotational temperature, have been obtained including both reactive and non-reactive collisions. The cross section sharply increases with translational energy up to a maximum and then decreases to an approximately flat trend. In figure 12a-b results for monoquantic de-excitation initiated from two different vibrational levels are shown for different rotational temperatures. Vibrational excitation emphasizes the peak value and shifts its position in the low energy region. The cross section dependence on the

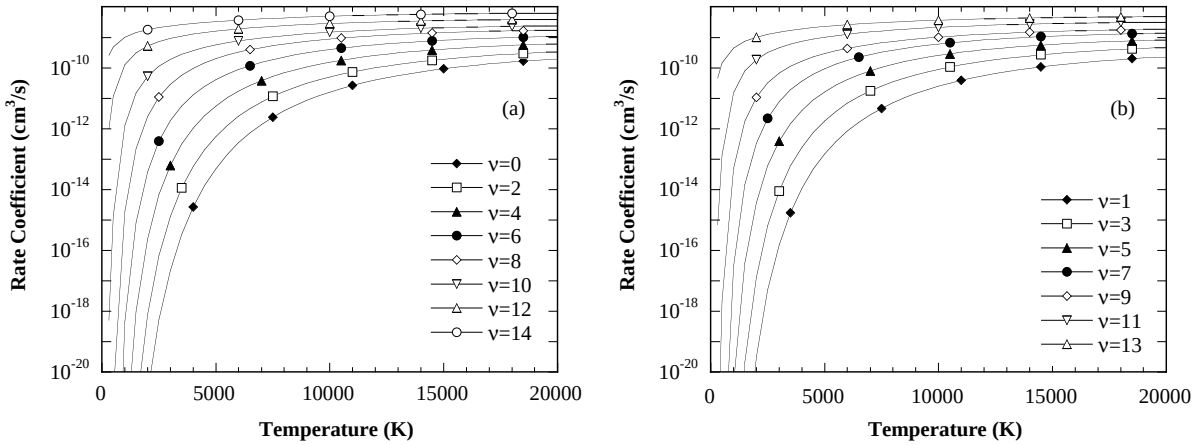

FIGURE 11. Dissociation rate coeffi cients averaged over Boltzmann distributions of rotational states plotted as a function of temperature for even (a) and odd (b) vibrational quantum numbers.

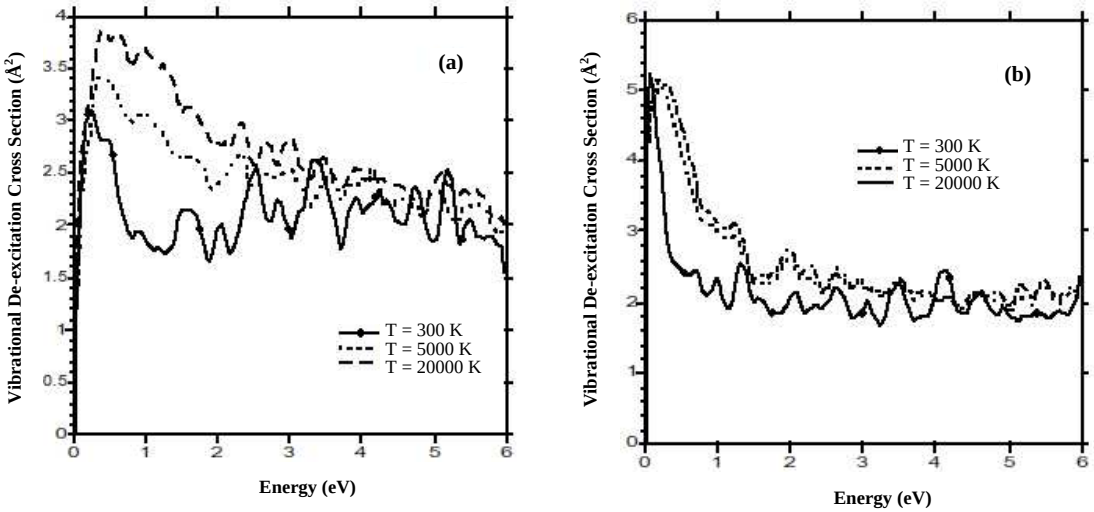

FIGURE 12. Monoquantic vibrational de-excitation cross sections as a function of translational energy, for different rotational temperatures. (a) v=5, (b) v=9.

rotational temperature is more significant for low initial v, due to the wide rotational ladder and to the related large contribution at high rotational temperature. Derived rate coefficients are in good agreement with the rates calculated by Laganá [22].

In order to compare the calculated dynamical data with experimental results, the global dissociation rate coefficient has been derived, building up a kinetic model of the H_2 dissociation as occurring in a thermal bath of atoms at a temperature T. The atomic hydrogen concentration is taken to be 100 times higher than that one of the molecules. As a consequence only V-T processes involving atomic hydrogen can be assumed to significantly contribute to populate the vibrational ladder. The kinetic problem deals with the solution of the vibrational master equation including 15 vibrational levels of H_2 submitted to the action of processes

$$H + H_2(v) \rightarrow H + H_2(v') \tag{16}$$

$$H + H_2(v) \rightarrow 3H \tag{17}$$

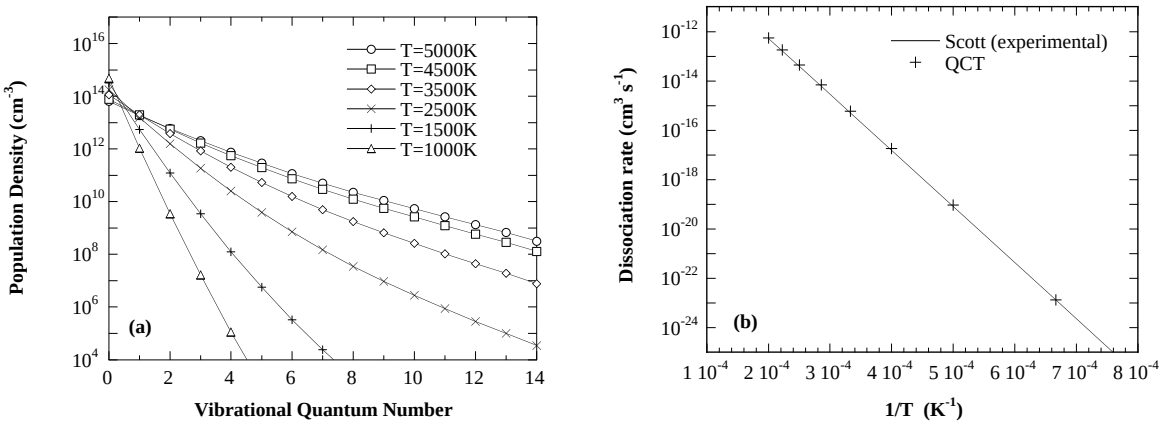

FIGURE 13. (a) Quasistationary vibrational distribution functions plotted versus vibrational quantum number for different gas temperature values. (b) A comparison of theoretical and experimental values of the global dissociation rate by Scott [23].

In this scheme the global dissociation rate is the resultant of the dissociative processes initiated from vibrationally excited molecules, expressed as

$$\nu_d = N_H \sum_{\nu} N_\nu K_d(\nu) = N_H N_{H_2} K_d \tag{18}$$

K_d, the second order dissociation constant, can be obtained from the relevant $K_d(\nu)$ values and from the vibrational distribution function N_ν. Vibrational populations have been determined by integration of the system of vibrational master equations, assuming the initial vibrational distribution as a delta function centered at ν=0 level.

The temporal evolution of vibrational populations can be followed up to the quasistationary condition. Quasistationary vibrational distributions have a markedly Boltzmann character at all translational temperatures and distortions occur only for high vibrational levels (figure 13a). In figure 13b the global dissociation constant is displayed as a function of $1/T$, the experimental global dissociation rates quoted in [23] is also reported, showing the good agreement between experimental and theoretical results and indirectly confirming both the accuracy of the potential energy surface and the reliability of the QCT approach.

SURFACE PROCESSES

The interaction of atomic and molecular hydrogen on the reactor walls is relevant in affecting the H_2 vibrational distribution through recombination/dissociation reactions and diffusion processes on the surface.

The recombination of atomic hydrogen on graphite has been studied in the framework of the semiclassical collisional method [24], according to which the dynamics of the chemical particles, H and H_2, interacting with the graphite surface is described classically by solving the relevant Hamilton's equations of motion while the phonons modes of the graphite surface are treated quantum-mechanically. The coupling between the classical degrees of freedom with the phonons dynamics is made via a time and surface temperature dependent effective potential V_{eff}, of the mean-field type.

The crystal model K62/62/62 consists of 186 carbon atoms displayed over three layers according to the appropriate lattice symmetry (figure 14a)

The adopted hydrogen-surface potential smoothly switches from H_2-graphite to H-graphite interaction potential according to the $H-H$ interatomic separation. H_2 is physisorbed on

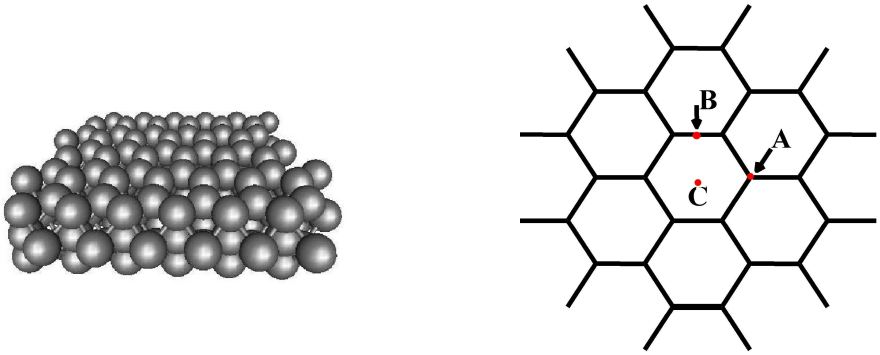

(a) (b)

FIGURE 14. (a) Crystal model K62/62/62. (b) Graphite surface structure.

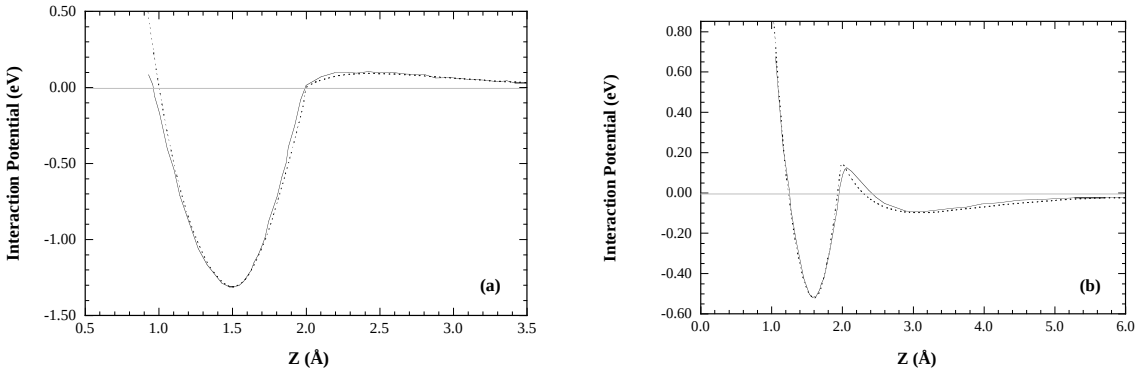

FIGURE 15. Hydrogen-surface interaction potential as a function of the atom surface distance, *Z*, at the site *A*. (a) ref. [27], (b) ref. [28]; dashed lines indicate fi tting curves.

graphite in the perpendicular geometry, as confirmed both by experimental and theoretical results [25, 26], the adsorption energy being negligible regardless the adsorption site. On the contrary the *H*-graphite interaction is characterized by chemiadsorption, the binding energy depending on the interacting site. Different semiempirical electronic structure calculations have been performed to explore the potential surface and it turns out that the strongest interaction occurs on top of carbon atom, i.e. at the lattice site *A* in figure 14b. The interaction potential for atomic hydrogen approaching the surface perpendicularly at site A has been modelled fitting results by Fromhertz et al. [27] (figure 15a) and by Jeloaica et al. [28] (figure 15b).
The more recent DFT calculations performed by Jeloaica et al. predict a well depth a factor two lower with respect to the value of ref. [27], affecting significantly the catalytic activity of the graphite surface. Reported results have been obtained employing the potential by Jeloaica et al.. Details on the parametric expressions for the interactions potentials can be found in refs. [29, 30]. Hydrogen recombination at graphite surface can occur through two alternative mechanisms:

- the direct Eley-Ridel two-step mechanism (*E-R mechanism*)

$$H_{gas} + graphite \rightarrow H_{ads} * graphite \tag{19}$$

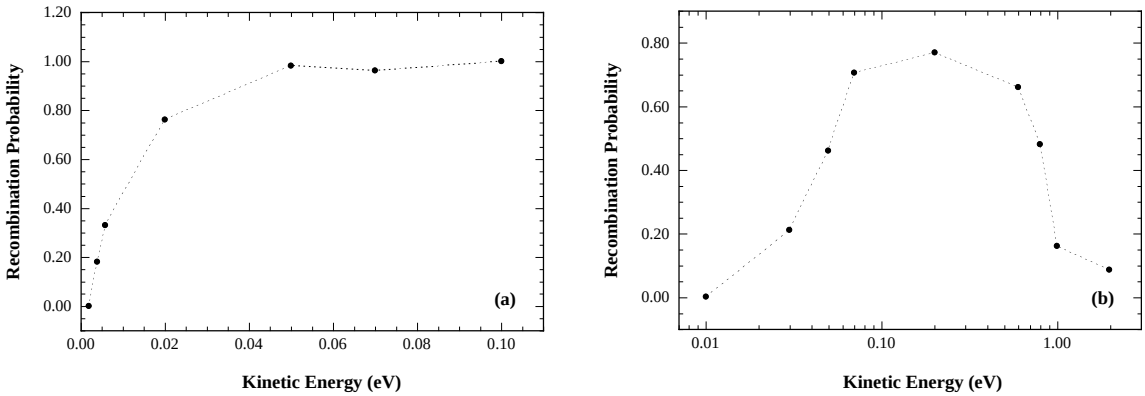

FIGURE 16. Recombination probability as a function of incident kinetic energy. (a) $T_S = 10K$; (b) $T_S = 500K$.

$$H_{ads} * graphite + H_{gas} \rightarrow H_2(v, j) + graphite \tag{20}$$

- the indirect Langmuir-Hinshelwood mechanism (*L-H mechanism*)

$$H_{ads} * graphite + H_{ads} * graphite \rightarrow H_2(v', j') + graphite \tag{21}$$

The L-H mechanism simulation of the diffusive processes of adsorbed hydrogen atoms across the surface is complex and requires the knowledge of the full topology of the interaction potential, therefore the E-R recombination reaction has been studied.

The adsorbed H atom is placed at the equilibrium distance of 1.5 Åand in thermal equilibrium with the surface at the temperature T_S, the molecular dynamic code simulates the H atom in the gas phase impinging on the surface with polar angles $(\theta;\phi)$ with a kinetic energy E_{kin}, giving the recombination probabilities, the nascent vibrational and rotational distribution of formed H_2 molecules and reaction probabilities for different reaction products.

Recombination probability critically depends on surface temperature: the increase of T_S corresponds to the decrease of the probability for the recombination. It can be appreciated by inspection of figure 16 where results for $T_S = 10K$ (temperature range for astrophysical applications) and for $T_S = 500K$ are presented. The energy distribution analysis shows that a fraction of the exothermic energy released in hydrogen recombination is shared among the internal states of the newly formed molecules, leading to non-Boltzmann nascent vibrational distribution, being the non-equilibrium character emphasized at high surface temperature. In figure 17 typical calculated vibrational populations of H_2 molecules for different surface temperatures are presented, at the impact energy of 0.03 eV.

The interaction with graphite actually can lead to activation of several reaction exit channels:

$$H_{ads} + H_{gas} \rightarrow \begin{array}{ll} H_2(v, j) & (a) \\ H_{gas} + H_{ads} & (b) \\ H_{gas} + H_{gas} & (c) \\ H_{ads} + H_{ads} & (d) \end{array} \tag{22}$$

the non-reactive surface processes (22)b-d are relevant in the investigation of plasma walls performance in fusion devices, in fact the relative importance with respect to the recombination channel can be considered as an indication of the efficiency of surface damage processes experimentally observed. Probabilities for reactive and non-reactive channels in hydrogen-graphite interaction are presented in figure 18.

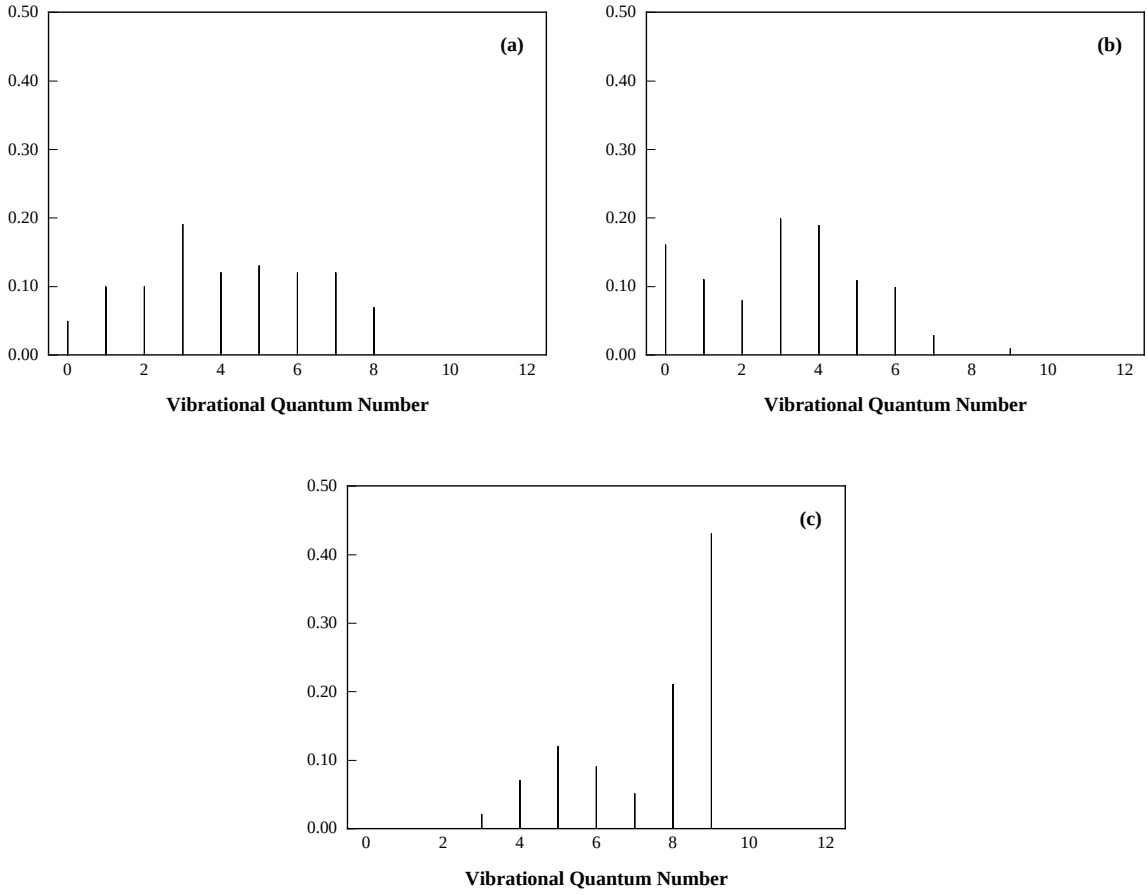

FIGURE 17. Population of vibrationally excited H_2 molecules in recombination process at the impact energy of 0.03 eV. (a) $T_S = 10K$; (b) $T_S = 100K$; (c) $T_S = 500K$.

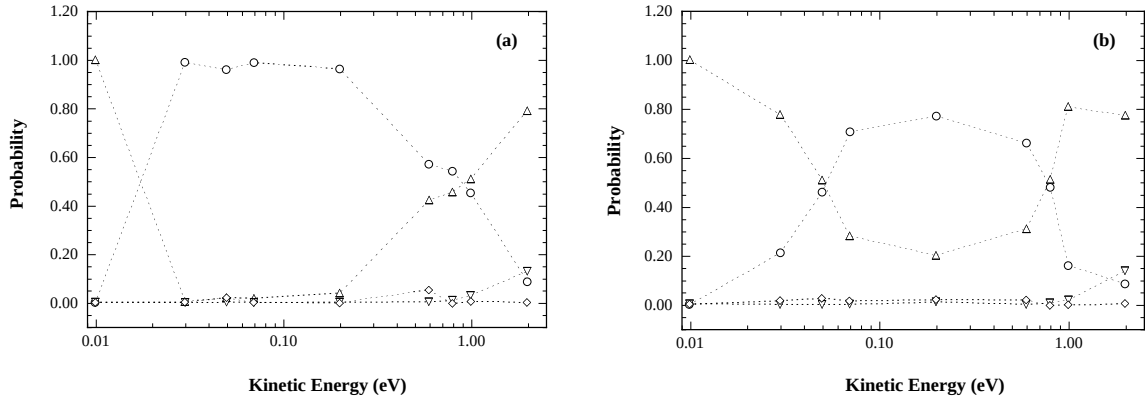

FIGURE 18. Probability for recombination (circles), adsorption of one atom (triangles), of both atoms (diamonds) and scattering of both atoms (down triangles) as a function of incident kinetic energy. (a) $T_S = 100K$; (b) $T_S = 500K$.

CONCLUSIONS

In the present report we have shown theoretical calculations of processes relevant to the modeling of negative ion sources. Emphasis has been given to the dependence of the process probability on the excitation of the internal degrees of freedom.

ACKNOWLEDGMENTS

This work has been partially supported by MIUR (Project No. 2003037912_010) and by ASI (contract I|R|055|02).

REFERENCES

1. M. Capitelli, R. Celiberto, and M. Cacciatore, in "Advanced in Atomic, Molecular and Optical Physics: Cross Section Data", edited by M. Inokuti, Academic Press, N.Y. and London, **33** (1994) 321.
2. R.K. Janev, in "Atomic and Molecular Processes in Fusion Edge Plasmas", edited by R.K. Janev, Plenum Press, N.Y. and London, (1995) 1.
3. J.N. Bardsley and J.M. Wadehra, Physical Review A **20** (1979) 1398.
4. J.M. Wadehra in "Nonequilibrium Vibrational Kinetics", edited by M. Capitelli, Springer-Verlag, New York and London, (1986).
5. C. Gorse, R. Celiberto, M. Cacciatore, A. Laganà and M. Capitelli, Chemical Physics **161** (1992) 211. C. Gorse, M. Bacal, R. Celiberto and M. Capitelli, Chemical Physics Letters **192** (1992) 161.
6. U. Fantz, B. Heger and D. Wünderlich, Plasma Physics Controlled Fusion **43** (2001) 1.
7. R. Celiberto, R.K. Janev, A. Laricchiuta, M. Capitelli, J.M. Wadehra and D.E. Atems, Atomic Data and Nuclear Data Tables **77** (2001) 161.
8. R. Celiberto and T.N. Rescigno, Physical Review A **47** (1993) 1939.
9. R. Celiberto, R.K. Janev and A. Laricchiuta, Physica Scripta **64** (2001) 26.
10. J.R. Hiskes, Journal of Applied Physics **51** (1980) 4592. J.R. Hiskes, Journal of Applied Physics **70** (1991) 3409.
11. R. Celiberto, A. Laricchiuta, U.T. Lamanna, R.K. Janev and M. Capitelli, Physical Review A, **60** (1999) 2091.
12. L.A. Pinnaduwage, W.X. Ding, D.L. McCorkle, S.H. Lin, A.M. Mebel and A. Garscadden, Journal of Applied Physics **85** (1999) 7064.
13. T.N. Rescigno and B.I. Schneider, Journal of Physics B **21** (1988) L691.
14. D.T. Stibbe and J. Tennyson, New Journal of Physics **1**, (1998) 21-29.
15. R. Celiberto, U.T. Lamanna, M. Capitelli, Physical Review A **50** (1994) 4778.
16. A. Laricchiuta, R. Celiberto, and R.K. Janev, Physical Review A **69** (2004) 022706.
17. F. Esposito, C. Gorse, M. Capitelli, Chemical Physics Letters **303** (1999) 636.
18. D.G. Truhlar, C.J. Horowitz, Journal of Chemical Physics **68** (1978) 2466; **71** (1979) 1514.
19. R.E. Roberts, R.B. Bernstein, C.F.Curtiss, Journal of Chemical Physics **50** (1969) 5163.
20. F. Esposito, PhD Thesis, Department of Chemistry, University of Bari (1999).
21. J.E. Dove, M.E. Mandy, Int. J. Chem. Kin. **18** (1986) 893.
22. A. Laganà, E. Garcia, "Quasiclassical rate coeffi cients for the $H + H_2$ reaction", University of Perugia, Italy (1996).
23. C.D. Scott, S. Fahrat, A. Gicquel, K. Hassouni, M. Lefebvre, J.Thermophysics and Heat Transfer **10** (1996) 426.
24. G.D. Billing, "Dynamics of molecule surface interactions", Wiley, New York (2000).
25. L. Mattera, F. Rosatelli, C. Salvo, F. Tommasini, U. Valbusa, G. Vidali, Surf. Sci. **93** (1980) 515.
26. D. Novaco, J. P. Wroblewski, Physical Review B **39** (1989) 11364.
27. T. Fromhertz, C. Mendoza, F. Ruette, Mon. Not. R. Astron. Soc. **263** (1993) 851.
28. L. Jeloaica, V. Sidis, Chemical Physics Letters **300** (1999) 157.
29. M. Rutigliano, M. Cacciatore and G.D. Billing, APID (Atomic and Plasma-Material Interaction Data for Fusion) **9** (2001) 267.
30. M. Rutigliano, M. Cacciatore and G.D. Billing, Chem.Phys.Lett. **340** (2001) 13.